

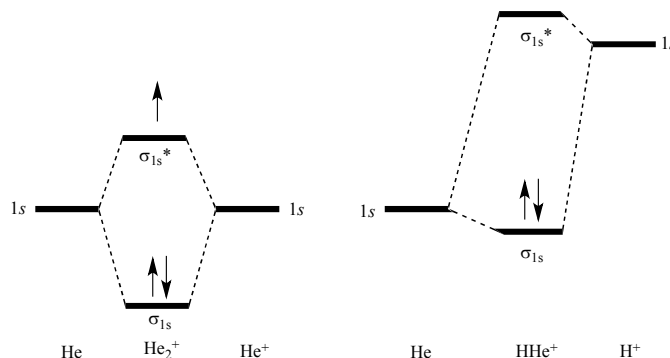
## CHAPTER 8: CHEMISTRY OF THE MAIN GROUP ELEMENTS

8.1	a.	$\text{H}_2$	74.2 pm	436 kJ/mol
		$\text{H}_2^+$	106 pm	255 kJ/mol

These values are consistent with the molecular orbital descriptions.  $\text{H}_2$  has two electrons in the bonding  $\sigma$  orbital,  $\text{H}_2^+$  has only one. The net attraction between the bonding electron and the nuclei are weaker in  $\text{H}_2^+$  relative to that between the two bonding electrons and the nuclei in  $\text{H}_2$ . Therefore, the bond distance is longer in  $\text{H}_2^+$ .

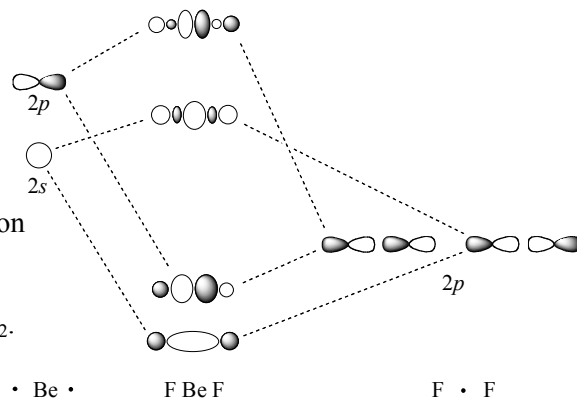
- b.  $\text{H}_3^+$  was described in Problems 5.21 and 5.43. It has a single pair of electrons in a 2-electron, 3-center bond, with bond orders of 1/3.

- 8.2  $\text{He}_2^+$  has 2 electrons in the bonding  $\sigma$  orbital and 1 in the antibonding  $\sigma^*$  orbital, with a bond order of  $1/2$ .  $\text{HeH}^+$  has a bond order of one, but with a poorer match between the energy levels of the two atoms ( $-13.6$  eV for H,  $-24.5$  for He).

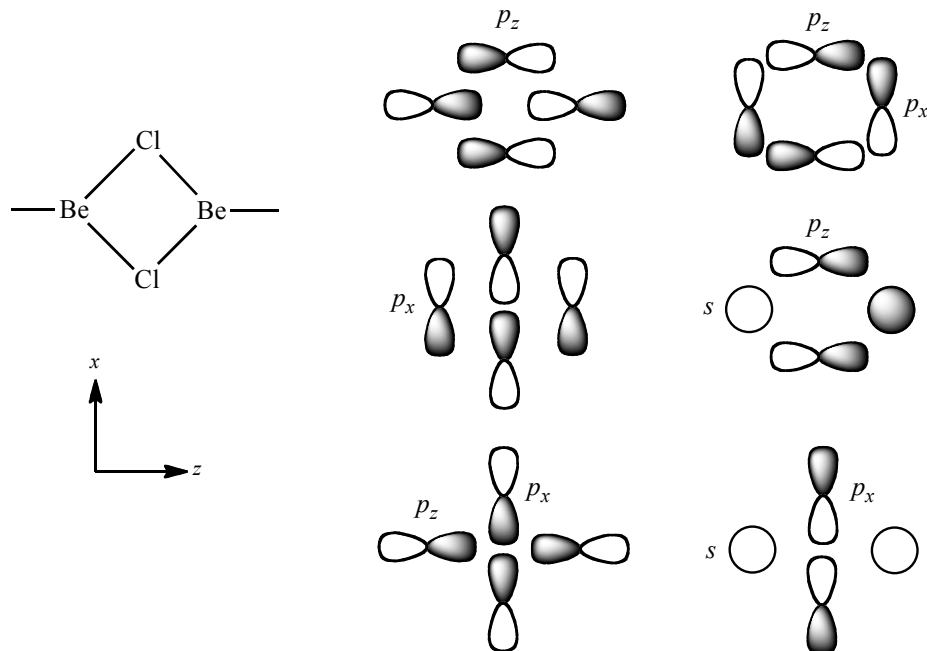


- 8.3 If the isoelectronic series could be continued, the ion  $\text{CsF}_4^+$  would be expected to have a similar structure to  $\text{XeF}_4$  and  $\text{IF}_4^-$ , with two lone pairs in *trans* positions. However, a variety of factors make such a species truly unlikely. For example, while the bonds in  $\text{XeF}_4$  and  $\text{IF}_4^-$  are best described as polar covalent, the tremendous difference in electronegativity between Cs and F suggest that ionic bonding would be necessary in  $\text{CsF}_4^+$ . However, complexes containing Cs(V) are unknown.
- 8.4 The equilibrium constants for formation of alkali metal ion complexes with cryptands are listed in Figure 8.7, with the formation constant for the sodium complex with cryptand [2.2.1] larger than for either the lithium or potassium complexes. A similar trend is found for the alkaline earths, with the maximum at strontium. Apparently the optimum size for an ion fitting in the cryptand is larger than sodium (atomic radius: 107 pm), but smaller than barium (149 pm) or potassium (138 pm), leaving strontium (132 pm) as the closest fit.

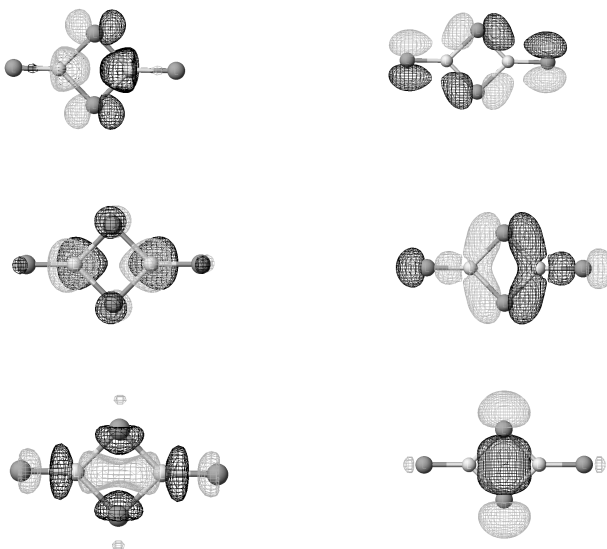
- 8.5 The diagram at the right shows the primary interactions forming molecular orbitals. The other orbitals on the fluorine atoms form lone-pair orbitals and  $\pi$  orbitals. The interactions are similar to those in carbon dioxide (Figure 5.25), but the poorer energy match between the valence orbitals leads to significantly less covalent character in the resulting bonds of  $\text{BeF}_2$ .



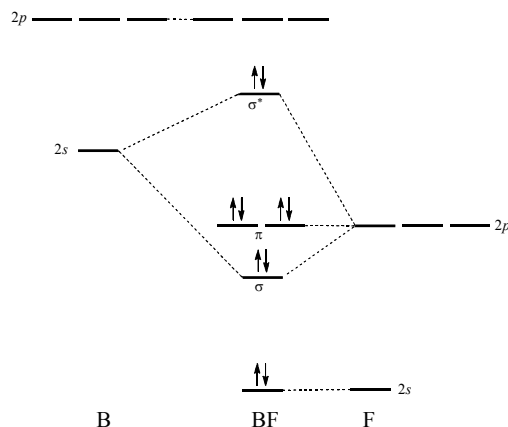
- 8.6 A combination of the in-plane  $p$  orbitals of Cl and the  $s$  and in-plane  $p$  orbitals of Be form orbitals that link the Be and Cl atoms in 3-atom, 2-electron bonds. The atomic orbital interactions that result in bonding molecular orbitals involving these bridging chlorine atoms are shown below. The antibonding orbitals also formed by these interactions, along with other orbitals with significant contribution from the terminal chlorine atoms, are not shown.



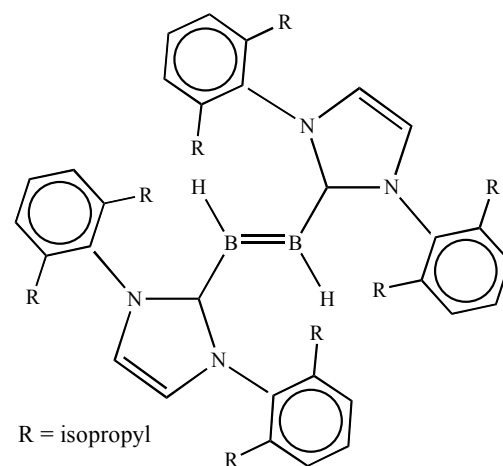
The same orbitals, shown as calculated using extended Hückel theory software, are below. Orbitals from the terminal chlorine atoms are included in these molecular orbitals.



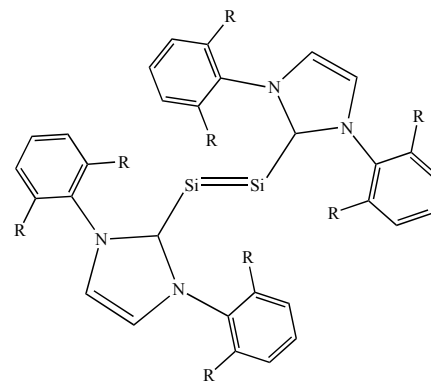
- 8.7** The much greater difference in orbital energies of B (−8.3 and −14.0 eV) and F (−18.7 and −40.2 eV) makes the BF bond weaker than that of CO. The *s* orbital of B and the *p* orbital of F can interact, but the *p*-*p* combination cannot interact significantly because of the large difference in *p* orbital energies. This mismatch results in weak single bonding, rather than the triple bond of CO.



- 8.8 a.** Evidence cited for a double bond includes an X-ray crystal structure that shows a very short boron–boron distance (156 pm) that is considerably shorter than compounds having boron–boron single bonds and comparable to the bond distance in compounds with double bonds between boron atoms. Density functional theory computations also showed a HOMO with boron–boron  $\pi$  bonding.



- b.** The product in this case was a silicon compound having a structure similar to the boron compound shown above, but lacking hydrogen atoms; nevertheless, it has bent geometry at the silicon atoms, leading to the zigzag structure shown at right. An X-ray crystal structure similarly shows a silicon–silicon distance consistent with a double bond, and density functional theory yields a HOMO with  $\pi$  bonding between the silicon atoms.



- 8.9** The combination of orbitals forming the bridging orbitals in  $\text{Al}_2(\text{CH}_3)_6$  is similar to those of diborane (Section 8.5.1). The difference is that the  $\text{CH}_3$  group has a *p* orbital (or  $sp^3$  hybrid orbital) available for bonding to the aluminum atoms, with the same symmetry possibilities as those of H atoms in  $\text{B}_2\text{H}_6$ .

## 8.10

$D_{2h}$	$E$	$C_2(z)$	$C_2(y)$	$C_2(x)$	$i$	$\sigma(xy)$	$\sigma(xz)$	$\sigma(yz)$	
$\Gamma(p_z)$	2	2	0	0	0	0	2	2	
$\Gamma(p_x)$	2	-2	0	0	0	0	2	-2	
$\Gamma(1s)$	2	0	0	2	0	2	2	0	
$A_g$	1	1	1	1	1	1	1	1	$z^2$
$B_{2g}$	1	-1	1	-1	1	-1	1	-1	$xz$
$B_{1u}$	1	1	-1	-1	-1	-1	1	1	$xy$
$B_{3u}$	1	-1	-1	1	-1	1	1	-1	$x$

Reduction of the representations  $\Gamma$  gives the following:

Boron orbitals:

a.  $\Gamma(p_z) = A_g + B_{1u}$

b.  $\Gamma(p_x) = B_{2g} + B_{3u}$

Hydrogen orbitals:

c.  $\Gamma(1s) = A_g + B_{3u}$

d. Treating each group orbital as a single orbital, the orbitals below have the indicated symmetries.

$D_{2h}$		$E$	$C_2(z)$	$C_2(y)$	$C_2(x)$	$i$	$\sigma(xy)$	$\sigma(xz)$	$\sigma(yz)$
$A_g(p_z)$		1	1	1	1	1	1	1	1
$B_{1u}(p_z)$		1	1	-1	-1	-1	-1	1	1
$B_{2g}(p_x)$		1	-1	1	-1	1	-1	1	-1
$B_{3u}(p_x)$		1	-1	-1	1	-1	1	1	-1
$A_g(s)$		1	1	1	1	1	1	1	1
$B_{3u}$		1	-1	-1	1	-1	1	1	-1

8.11 Carbon has two lone pairs in  $C(PPh_3)_2$ , with VSEPR predicting a tetrahedral electron group geometry. The bulky phenyl groups limit the impact of the nonbonding pairs and force a larger angle.

**8.12** The cations of  $\text{CaC}_2$ ,  $\text{CeC}_2$ , and  $\text{YC}_2$  are not isoelectronic. While  $\text{Ca}^{2+}$  has no valence electrons, the unusual 2+ group 3 ion  $\text{Y}^{2+}$  and the lanthanide  $\text{Ce}^{2+}$  contain 1 and 2 valence electrons, respectively. It has been suggested (Greenwood and Earnshaw, *Chemistry of the Elements*, 2<sup>nd</sup> ed., p. 299) that there is some transfer of this valence electron density to the  $\pi^*$  orbitals of the dicarbide (or acetylide) ion, resulting in a longer bond.

**8.13** Radioactive decay obeys a first order kinetic equation:

$$\frac{dx}{dy} = -kx; \quad \ln\left(\frac{x}{x_0}\right) = -kt$$

The relationship of the half-life (the time at which  $x = \frac{1}{2} x_0$ ) and the rate constant is

$$\ln\left(\frac{x}{x_0}\right) = \ln\left(\frac{1}{2}\right) = -kt_{1/2} = -0.693$$

$$k = \frac{0.693}{t_{1/2}}$$

$$k = \frac{0.693}{t_{1/2}} = 1.21 \times 10^{-4} \text{ y}^{-1}$$

$$\ln\left(\frac{x}{x_0}\right) = \ln(.56) = -1.21 \times 10^{-4} t$$

$$t = 4.8 \times 10^3 \text{ y}$$

**8.14**  $I_h$  symmetry includes 12  $C_5$  axes, 12  $C_5^2$  axes, 20  $C_3$  axes, 15  $C_2$  axes, an inversion center, 12  $S_{10}$  axes, 20  $S_6$  axes, and 15 mirror planes. One of the  $C_5$  axes and an  $S_{10}$  axis can be seen in the middle of the second fullerene figure (end view) in Figure 8.18. There are six of each of these, each representing two rotation axes,  $C_5$  and  $C_5^4$ , for a total of 12. The same axes fit the 12  $S_5^2$  axes. If the structure is rotated to line up two hexagons surrounded by alternating pentagons and hexagons, the 20  $C_3$  and 20  $S_6$  axes can be seen (one in the center, three in the first group around that hexagon, and three adjacent pairs in the next group, doubled because of  $C_3$  and  $C_3^2$ ). The  $C_2$  axes pass through bonds shared by two hexagons, with pentagons at each end. These original hexagons each have two more, making five, the next ring out has eight, and the perimeter (seen edge on) has two for a total of 20  $C_2$ . There are five mirror planes through the center of the pentagons surrounded by five hexagons (see the end view of Figure 8.18 again), and there are three sets of these for a total of 15. (All this is best seen using a model!)

**8.15** a.  $T_d$

b.  $I_h$

c.  $D_{5h}$

d. zigzag:  $C_{2h}$       armchair:  $D_{2h}$

- 8.16** Graphane, obtained from the hydrogenation of graphene, was first reported in 2009 (see J. Agbenyega, *Mater. Today*, **2009**, 12, 13), and research interest has grown rapidly.
- 8.17** Printing on transparencies is suggested for this exercise. Rolling up of the diagram should show that more than one chiral form is possible.
- 8.18** Readers are encouraged to search for the most recent references in this promising area. At this writing (February 2013) the reference has been cited in 176 other articles in scientific journals.
- 8.19** The reference provides absorption spectra and colors of solutions containing mixtures of armchair-enriched single-walled carbon nanotubes with different diameters, ranging from 0.83 nm to 1.5 nm. The strongest absorption band for the nanotubes shifted to longer wavelength (lower energy) as the diameter increased, with the smallest absorbing at 407 nm and the largest at 785 nm, and the observed colors (complementary to the colors of the strongest absorption bands) changed accordingly. The observations were consistent with the energy levels of the nanotubes becoming closer as the diameters of the tubes increased. A similar size effect is observed for quantum dots (Section 7.3.2).
- 8.20** The increased stability of 2+ oxidation states as compared to 4+ is an example of the “inert pair” effect (see Greenwood and Earnshaw, *Chemistry of the Elements*, 2<sup>nd</sup> ed., pp. 226, 227, 374). In general, the ionization energy decreases going down a column of the periodic table, because of greater shielding by the inner electrons. In this family, removal of the second electron is fairly easy, as it is the first in the higher-energy *p* orbitals. However, the next two electrons to be removed are the *s* electrons, and they are not as thoroughly shielded in the ions. The effect is larger for the three lower members of the group because the *d*<sup>10</sup> electrons are added between the *s* and *p* electrons. The lower electronegativity of C and Si make them more likely to form covalent bonds than ions.
- 8.21 a.** H<sub>2</sub>ISiSiH<sub>2</sub>I has a C<sub>2</sub> axis perpendicular to the plane of the diagram as drawn, a perpendicular mirror plane (the plane of the diagram), and an inversion center, C<sub>2h</sub>.

- b.** The Si—H stretches have the reducible representation shown below, which reduces to  $\Gamma = A_g + B_g + A_u + B_u$ . *A<sub>u</sub>* and *B<sub>u</sub>* are IR-active.

C <sub>2h</sub>	<i>E</i>	C <sub>2</sub>	<i>i</i>	σ <sub>h</sub>	
Γ	4	0	0	0	
<i>A<sub>g</sub></i>	1	1	1	1	<i>R<sub>z</sub></i>
<i>B<sub>g</sub></i>	1	-1	1	-1	<i>R<sub>x</sub>, R<sub>y</sub></i>
<i>A<sub>u</sub></i>	1	1	-1	-1	<i>z</i>
<i>B<sub>u</sub></i>	1	-1	-1	1	<i>x, y</i>

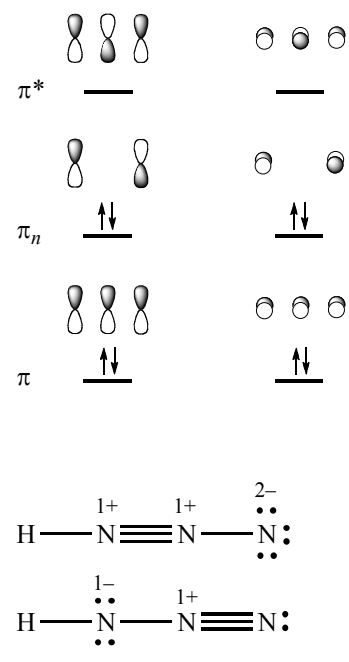
- 8.22** P<sub>4</sub> (g)  $\rightleftharpoons$  2 P<sub>2</sub> (g), Δ*H* = 217 kJ mol<sup>-1</sup>  
P<sub>4</sub> has six P—P bonds, so six bonds are broken and two triple bonds are formed.

$$\Delta H = \Sigma \text{bond dissociation energy (reactant)} - \Sigma \text{bond dissociation energy (product)}$$

$$217 = 6 \times 200 - 2(\text{bond dissociation energy of P}\equiv\text{P})$$

$$\text{Bond dissociation energy of P}\equiv\text{P} = 492 \text{ kJ mol}^{-1}$$

The *p*<sub>π</sub> orbitals in P<sub>2</sub> do not overlap as effectively as those in N<sub>2</sub> on the basis of the larger atomic radius of P relative to N, resulting in weaker π bonds in P<sub>2</sub>.

- 8.23**
- a.**  $\text{N}_3^-$  has molecular orbitals similar to those of  $\text{CO}_2$  (Section 5.4.2), with two occupied  $\sigma$  orbitals and two occupied  $\pi$  orbitals for a total of four bonds. In contrast to the situation in  $\text{CO}_2$ , the atomic orbitals involved in the bonding in  $\text{N}_3^-$  have equal energies.
- b.** Because the HOMOs of  $\text{N}_3^-$  (at right) are primarily composed of  $p$  orbitals of the terminal nitrogen atoms,  $\text{H}^+$  bonds at an angle to the  $\text{N}=\text{N}=\text{N}$  axis. The angle is  $114^\circ$ , larger than the  $90^\circ$  predicted by simple bonding to a  $p$  orbital.
- c.** The  $\text{H}-\text{N}-\text{N}$  angle is  $114^\circ$ . This observation suggests that the first resonance structure (with an  $\text{N}(sp)-\text{H}$  bond) contributes less to the electronic ground state of  $\text{HN}_3$  relative to the second structure (with an  $\text{N}(sp^3)-\text{H}$  bond). A decreased terminal  $\text{N}-\text{N}$  distance relative to the central  $\text{N}-\text{N}$  distance is consistent with these contributions.
- 
- The diagrams show the atomic orbitals (AOs) and molecular orbitals (MOs) for  $\text{N}_3^-$ . On the left, the MOs are labeled  $\pi^*$ ,  $\pi_n$ , and  $\pi$ . On the right, the MOs are labeled  $\pi^*$ ,  $\pi_n$ , and  $\pi$ . The  $\pi_n$  MOs are occupied by two electrons each, indicated by  $\uparrow\downarrow$ . The  $\pi$  MO is also occupied by two electrons. The  $\pi^*$  MOs are empty. The resonance structures for  $\text{HN}_3$  are shown below the text. The first structure is  $\text{H}-\overset{1+}{\text{N}}\equiv\overset{1+}{\text{N}}-\overset{2-}{\text{N}}$  with lone pairs on the terminal nitrogens. The second structure is  $\text{H}-\overset{1-}{\text{N}}-\overset{1+}{\text{N}}\equiv\text{N}$  with lone pairs on the terminal nitrogens.

- 8.24** The electronegativity of H (2.300) is less than that of N (3.066). Hydrazine has two hydrogen atoms and an equally electronegative  $\text{NH}_2$  group bound to each nitrogen atom, while ammonia has three hydrogens bound to N. In this way, ammonia features three polar covalent bonds enriching the electron density at nitrogen, while hydrazine features two polar covalent  $\text{N}-\text{H}$  bonds and one nonpolar covalent bond (to the  $\text{NH}_2$  group). The N of ammonia is therefore more electron-rich, and hydrazine is the weaker aqueous base.

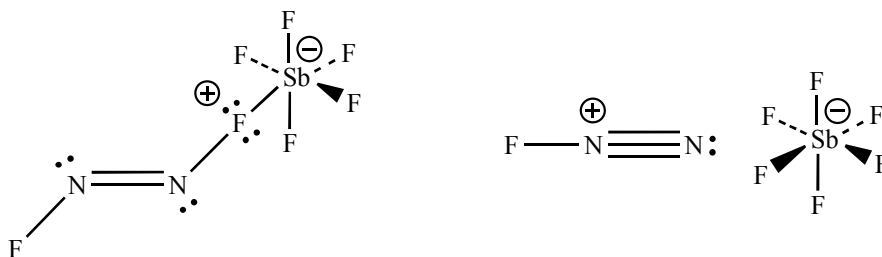
Another factor is the potential for hydrogen bonding with water in the resulting conjugate acids. An ammonium ion ( $\text{NH}_4^+$ ) features four excellent hydrogen bond donors per N atom, while hydrazinium ion features just three hydrogen atoms bound to a positively charged N atom. The enhanced opportunities for  $\text{NH}_4^+$  solvation relative to  $\text{N}_2\text{H}_5^+$  contribute to  $\text{NH}_3$  being a stronger base.

- 8.25** The larger central atoms feature longer bond lengths, leading to lower concentrations of bonding electron density close to the Group 15 atom, reducing bonding pair-bonding pair repulsion. The lone pair subsequently exerts increasing influence down the column, forcing smaller angles as the atomic radius of the central atom increases. This decrease in bonding pair-bonding pair repulsion can also be explained using electronegativity arguments, with the most electronegative nitrogen atom drawing a larger share of the bonding electron density towards it relative to the other group 15 elements that progressively become less electronegative down the column.
- 8.26** One  $p$  orbital of each oxygen is used for the  $\sigma$  bond to nitrogen, and the  $p$  orbital perpendicular to the plane of the molecule is used for a  $\pi$  orbital. The remaining  $p$  orbital is in the plane of the molecule, so addition of a proton to this lone pair leaves the entire molecule planar.

- 8.27** From Table 8.10

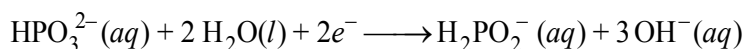
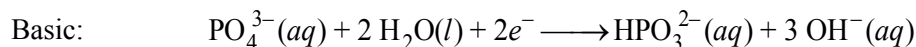
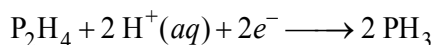
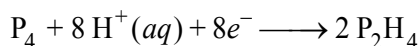
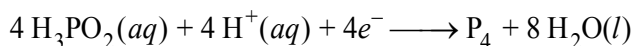
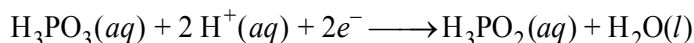
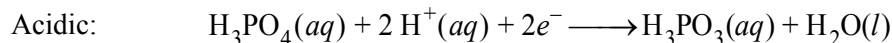
$\text{N}_2\text{O}$	$C_{\infty v}$	$\text{NO}$	$C_{\infty v}$	$\text{NO}_2$	$C_{2v}$	$\text{N}_2\text{O}_3$	$C_s$
$\text{N}_2\text{O}_4$	$D_{2h}$	$\text{N}_2\text{O}_5$	$D_{2h}$	$\text{NO}^+$	$C_{\infty v}$	$\text{NO}_2^+$	$D_{\infty h}$
$\text{NO}_2^-$	$C_{2v}$	$\text{NO}_3^-$	$D_{3h}$	$\text{N}_2\text{O}_2^{2-}$	$C_{2h}$	$\text{NO}_4^{3-}$	$T_d$
$\text{HNO}_2$	$C_s$	$\text{HNO}_3$	$C_s$				

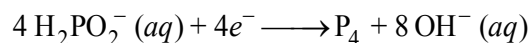
- 8.28 a. Computational work suggests that the electronic ground state of *cis*-N<sub>2</sub>F<sub>4</sub> is 1.4 kcal/mol lower than that of *trans*-N<sub>2</sub>F<sub>4</sub> at 298 K.
- b. Two *trans-cis* isomerization mechanisms are proposed. The simpler mechanistic possibility involves rotation about the N=N bond. A lower limit of 59.6 kcal/mol was calculated for this isomerization mechanism. The second possibility proceeds via a planar transition state that resembles [N<sub>2</sub>F]F, with relatively short and long N—F bonds, and a nitrogen–nitrogen triple bond, respectively. The transformation of nitrogen–nitrogen π bonding electron density to nonbonding electron density at nitrogen completes the isomerization. An activation barrier of 68.7 kcal/mol was determined for this mechanism. The activation barrier for isomerization via N=N rotation is 9.1 kcal/mol less than the proposed barrier for the [N<sub>2</sub>F]F mechanism.
- c. As a strong Lewis acid, SbF<sub>5</sub> can engage in a donor-acceptor interaction with a nonbonding pair on a fluorine atom (left). The structure on the right, where the F atom has been completely transferred, resulting in [N<sub>2</sub>F][SbF<sub>6</sub>], is the limiting result of this interaction.



While fluoride transfer is not envisioned to occur when SbF<sub>5</sub> assists in the isomerization, this possibility is instructive since it suggests that the interaction on the left is expected to lengthen one N—F bond while shortening the other N—F bond and the N—N bond. These changes are predicted to lower the activation barrier of the donor-acceptor complex (left) towards formation of the planar isomerization transition state that resembles [N<sub>2</sub>F]F, with a relatively short and long N—F bonds, and a nitrogen–nitrogen triple bond, respectively.

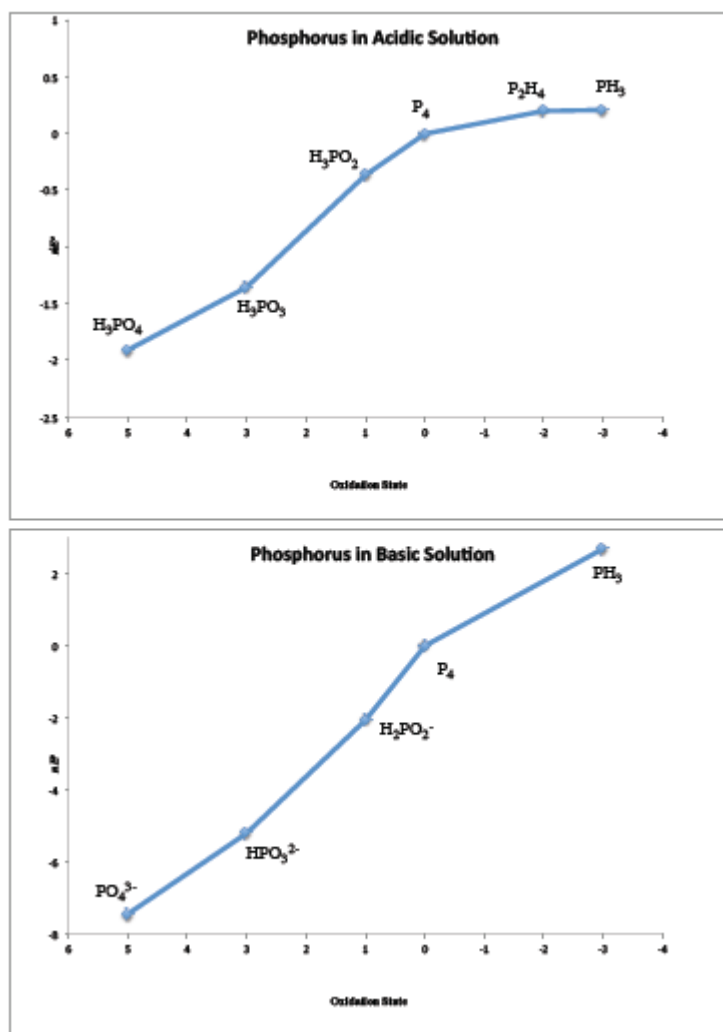
- 8.29 The balanced reduction half-reactions, for acidic and basic conditions, respectively, follow.



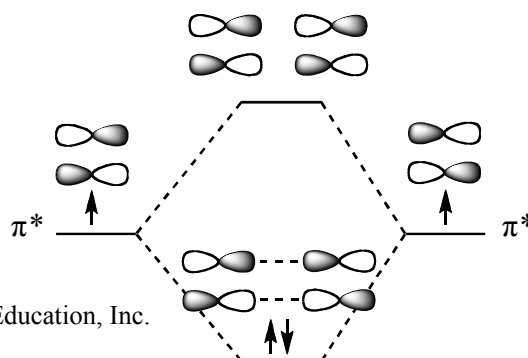


The Frost diagram for phosphorus in acidic solution features points at (5, -1.915;  $\text{H}_3\text{PO}_4$ ), (3, -1.363;  $\text{H}_3\text{PO}_3$ ), (1, -0.365;  $\text{H}_3\text{PO}_2$ ), (0, 0;  $\text{P}_4$ ), (-2, 0.200;  $\text{P}_2\text{H}_4$ ), and (-3, 0.206;  $\text{PH}_3$ ).

The Frost diagram for phosphorus in basic solution features points at (5, -7.43;  $\text{PO}_4^{3-}$ ), (3, -5.19;  $\text{HPO}_3^{2-}$ ), (1, -2.05;  $\text{H}_2\text{PO}_2^-$ ), (0, 0;  $\text{P}_4$ ), (-3, 2.67;  $\text{PH}_3$ ).



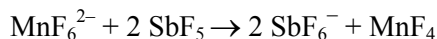
- 8.30** The bonding between  $\text{O}_2$  units is proposed to involve interactions between the singly occupied  $\pi^*$  orbitals of neighboring molecules. Such interactions would generate both bonding and antibonding molecular orbitals, with the



originally unpaired  $\pi^*$  electrons stabilized (*i.e.*, lowered in energy) as they occupy the bonding orbitals in  $O_8$ . One such interaction is shown at right. Diagrams of the four highest occupied molecular orbitals of  $O_8$  (which may be viewed as  $(O_2)_4$ ) are in the reference.

**8.31**  $S_2$  is similar to  $O_2$ , with a double bond. As a result, the bond is shorter than single bonds in  $S_8$ .

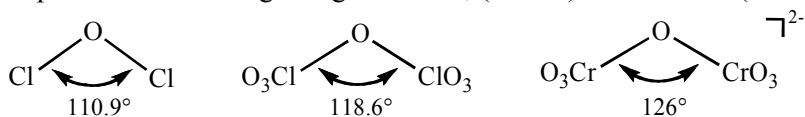
**8.32**  $MnF_6^{2-}$  acts as a Lewis base, transferring two  $F^-$  ions to two  $SbF_5$  molecules:



The  $MnF_4$  intermediate can then lose an F atom, with two of these radicals coupling to form  $F_2$ :



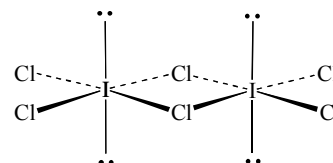
**8.33 a.** Although the  $ClO_3$  groups in  $Cl_2O_7$  are highly electronegative, their size is apparently responsible for the larger angle in  $Cl_2O_7$  ( $118.6^\circ$ ) than in  $Cl_2O$  ( $110.9^\circ$ ).



**b.** In the dichromate ion the highly electropositive Cr atoms allow the central oxygen to attract electrons more strongly than is possible in  $Cl_2O_7$ , resulting in stronger bonding pair-bonding pair repulsions around the central oxygen in  $[Cr_2O_7]^{2-}$  and a larger bond angle ( $126^\circ$ ).

**8.34**  $I_3^-$  is linear because there are three lone pairs in a trigonal geometry on the central I.  $I_3^+$  is bent because there are only two lone pairs on the central I.

**8.35** B has only three valence electrons. Adding six from the hydrogen atoms gives  $B_2H_6$  a total of 12 electrons. The 3-center 2-electron bonds result in four pairs around each boron atom and nearly tetrahedral symmetry at each boron atom. Iodine has seven valence electrons initially. In  $I_2Cl_6$ , five more are added to each iodine, resulting in 12 electrons and octahedral geometry around each iodine.



**8.36**  $F^- + BrF_3 \rightarrow BrF_4^-$        $KF$  acts as a base;  $BrF_4^-$  is the solvent anion.

$SbF_5 + BrF_3 \rightarrow BrF_2^+ + SbF_6^-$        $BrF_2^+$  is the cation of the solvent;  $SbF_5$  acts as the acid.

**8.37 a.**  $Br_2^+$  and  $I_2^+$  have one less antibonding electron than  $Br_2$  and  $I_2$ , so the cations have bond orders of 1.5 and shorter bonds than the neutral molecules:

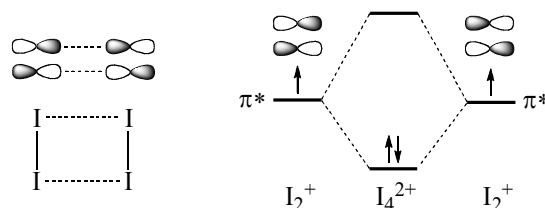
	Bond Order	Bond Distance (pm)		Bond Order	Bond distance (pm)
$Br_2$	1.0	228	$I_2$	1.0	267
$Br_2^+$	1.5	213	$I_2^+$	1.5	256

**b.** The most likely transition is from the  $\pi_g^*$  (HOMO) to  $\sigma_u^*$  (LUMO) (see Figure 5.7 for comparable energy levels of  $F_2$ ). Because the observed colors are complementary to the colors absorbed,  $Br_2^+$  is expected to absorb primarily green light, and  $I_2^+$  is expected to absorb primarily orange light. Because orange light is less energetic than green,  $I_2^+$  has

the more closely spaced HOMO and LUMO.

- c. In both  $I_2$  and  $I_2^+$  the HOMO and LUMO are the  $\pi_g^*$  and  $\sigma_u^*$ , respectively.  $I_2$  absorbs primarily yellow light (to give the observed violet color) and  $I_2^+$  absorbs primarily orange (to give blue). Because yellow light is more energetic than orange,  $I_2$  has the more widely spaced HOMO and LUMO.

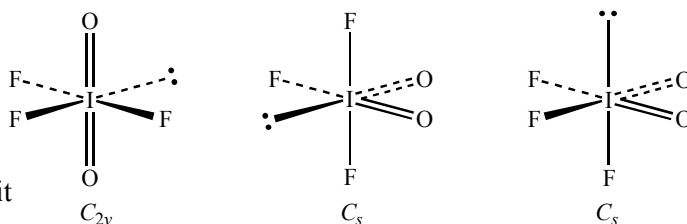
- 8.38 a. In  $I_2^+$  there are three electrons in the  $\pi^*$  orbitals that result from interactions between  $5p$  orbitals (these are the orbitals labeled  $4\pi_g^*$  in Figure 6.10). Interaction between the singly occupied  $\pi^*$  orbitals of two  $I_2^+$  ions can lead to stabilization of electrons by formation of a bonding molecular orbital that can connect the  $I_2^+$  units when  $I_4^{2+}$  is formed.



- b. Higher temperature would provide the energy to break the bonds between the  $I_2^+$  units and favor the monomer. In addition, formation of two  $I_2^+$  ions from  $I_4^{2+}$  would be accompanied by an increase in entropy, also favoring the monomer at higher temperatures.

- 8.39 There are three possibilities:

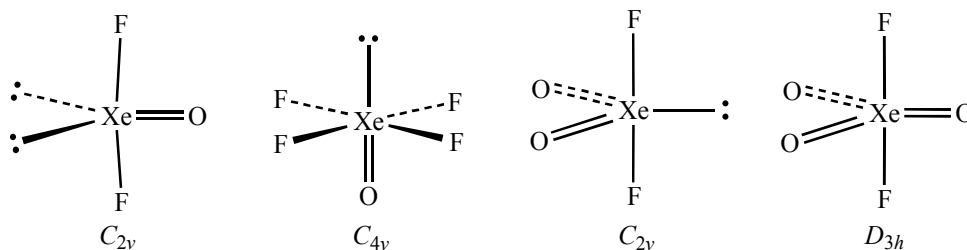
The third structure, with the lone pair and double bonds in a facial arrangement, is least likely because it would have the greatest degree of electron-electron repulsions involving these regions of high electron concentrations.



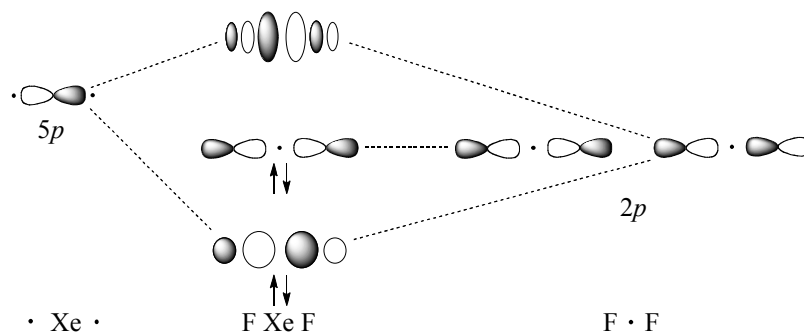
Infrared data can help distinguish between the other two structures. In the first structure, only the antisymmetric stretch would be IR-active, giving a single absorption band. In the second structure, both the symmetric and antisymmetric stretches would be IR-active, giving two bands. Observation of two I–O bands is therefore consistent with the second structure. This structure, which has fewer  $90^\circ$  lone pair–double bond repulsions than the first structure, is also most likely by VSEPR considerations. Other experimental data are also consistent with the second structure.

- 8.40 Superhalogens are species which, like the halogens, have very high electron affinities. Classic superhalogens contain a central atom surrounded by highly electronegative atoms or groups of atoms. Examples include  $MnO_4$ ,  $AlCl_4^-$ , and  $BO_2^-$ . See K. Pradhan, G. L. Gutsev, P. Jena, *J. Chem. Phys.*, **2010**, *133*, 144301; C. Sikorska, P. Skurski, *Inorg. Chem.*, **2011**, *50*, 6384; and references cited therein.
- 8.41 These reactions take place in the gas phase. The initial product of Xe with  $PtF_6$  is believed to be  $Xe^+ PtF_6^-$ ; however, when these two ions are in close proximity, they may react further to give  $[XeF]^+$ ,  $[Pt_2F_{11}]^-$ , and other products.  $SF_6$ , if present in large excess, prevents the formation of these secondary products, apparently by acting as an inert diluent and preventing effective collisions between the desired products.

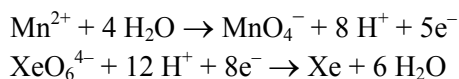
8.42



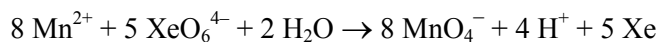
8.43 Two electrons are in the bonding orbital and two are in the nonbonding orbital:

8.44 Xe(OTeF<sub>5</sub>)<sub>4</sub>: The OTeF<sub>5</sub> group has one electron available for bonding on the O, so the four groups form a square planar structure around Xe, with lone pairs in the axial positions.O=Xe(OTeF<sub>5</sub>)<sub>4</sub>: A square pyramidal structure, with O in one of the axial positions and a lone pair on the other, and OTeF<sub>5</sub> groups in the square base.

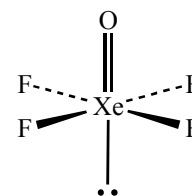
8.45 Half reactions:



Overall reaction:

8.46 XeF<sub>5</sub><sup>-</sup> has  $D_{5h}$  symmetry. The reducible representation for Xe–F stretching is

$D_{5h}$	$E$	$2C_5$	$2C_5^2$	$5C_2$	$\sigma_h$	$2S_5$	$2S_5^3$	$5\sigma_v$
$\Gamma$	5	0	0	1	5	0	0	1

, which reduces to  $\Gamma = A_1' + E_1' + E_2'$ , with only  $E_1'$  IR-active.

8.47 a. Point group:  $C_{4v}$

$C_{4v}$	$E$	$2C_4$	$C_2$	$2\sigma_v$	$2\sigma_d$	
$\Gamma$	18	2	-2	4	2	
$A_1$	1	1	1	1	1	$z$
$A_2$	1	1	1	-1	-1	$R_z$
$B_1$	1	-1	1	1	-1	
$B_2$	1	-1	1	-1	1	
$E$	2	0	-2	0	0	$(x, y), (R_x, R_y)$

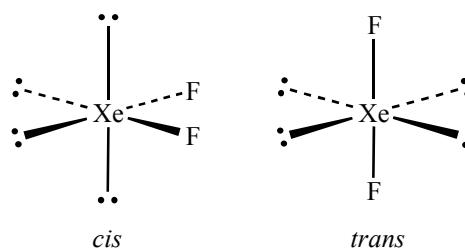
b.  $\Gamma = 4A_1 + A_2 + 2B_1 + B_2 + 5E$

c. Translation:  $A_1 + E$  (match  $x, y$ , and  $z$ )

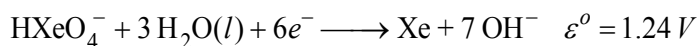
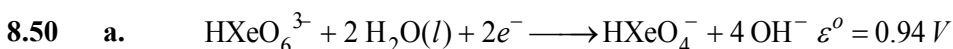
Rotation:  $A_2 + E$  (match  $R_x, R_y$ , and  $R_z$ )

Vibration: all that remain:  $3A_1 + 2B_1 + B_2 + 3E$

8.48 By the VSEPR approach,  $\text{XeF}_2^{2-}$  would be expected to have a steric number of 6, with four lone pairs on xenon. Two structures, *cis* and *trans*, need to be considered. In the *cis* structure there would be five lone pair-lone pair interactions at  $90^\circ$ , and in the *trans* structure there would be only four such interactions. The *trans* structure, therefore, would be expected to be more likely. However, the number of lone pair-lone pair repulsions would still be high, likely making this a difficult ion to prepare.



8.49 The energy necessary for vibrational excitation decreases with reduced mass; consequently, the lowest energy band, at  $1003.3 \text{ cm}^{-1}$ , is assigned to the Xe-D stretch of  $\text{DXeOXeD}$ , the deuterium analogue of  $\text{HXeOXeH}$ . The remaining unassigned bands, at  $1432.7$  and  $1034.7 \text{ cm}^{-1}$ , are therefore due to the Xe-H and Xe-D stretches, respectively, of  $\text{HXeOXeD}$ , which is also formed.



b. The disproportionation reaction of interest is:



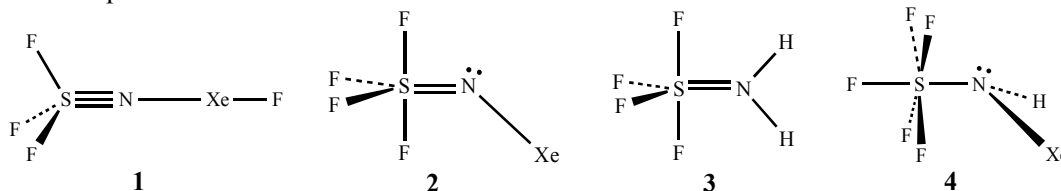
$\Delta G^\circ = -nFE^\circ = -(6 \text{ mol})(96485 \frac{\text{C}}{\text{mol}})(0.30 \frac{\text{J}}{\text{C}}) = -1.7 * 10^5 \text{ J} (-170 \text{ kJ}).$

8.51 a. The synthesis of  $\text{XeO}_2$  is very challenging to carry out. A special reactor composed of a perfluoro-ethylene/propylene copolymer must be rendered completely moisture free by extended treatment under vacuum. The reactivity of the container surface is then further reduced by treatment with  $\text{F}_2$  gas. Once the container is prepared, a small volume of water is added in an Ar gas atmosphere, and cooled to  $0^\circ \text{C}$ . The reaction is initiated by

slowly adding  $\text{XeF}_4$  crystals. The authors emphasize the importance of both the order of the addition (water first, then  $\text{XeF}_4$ ) and the speed of addition. The large and negative reaction  $\Delta H$ , coupled with the relatively small volume of solvent to dissipate the heat, can result in complications, including decomposition of the product; the mixture must be kept at  $0^\circ\text{C}$ . Within 30 seconds after mixing, yellow  $\text{XeO}_2$  precipitates from the solution. The  $\text{XeO}_2$  solid is then separated from the reaction mixture via centrifugation of the mini-reactor itself at  $0^\circ\text{C}$ . The resulting solid is thermally unstable at ambient temperature and must be kept cold ( $-78^\circ\text{C}$ ) for long-term storage.

- b. VSEPR theory predicts monomeric  $\text{XeO}_2$  to be a bent molecule with a persistent dipole moment that should permit solubility in water. The insolubility of obtained  $\text{XeO}_2$  samples suggests an extended  $\text{XeO}_2$  structure; individual monomeric units apparently do not persist in water.
- c. Application of isotopically labeled water in the synthesis facilitated  $\text{XeO}_2$  characterization. The presence of exclusively  $\text{Xe}-\text{O}$  bonding was inferred by preparing  $\text{XeO}_2$  as described in (a) using  $\text{H}_2^{16}\text{O}$  and  $\text{H}_2^{18}\text{O}$ , respectively. The Raman spectrum of the  $\text{H}_2^{16}\text{O}$ -derived  $\text{XeO}_2$  was identical to that of the  $\text{H}_2^{18}\text{O}$ -derived  $\text{XeO}_2$  sample, except that all of the bands of the  $\text{H}_2^{16}\text{O}$ -derived  $\text{XeO}_2$  sample were shifted to slightly higher energies. The identical spectral patterns, coupled with an isotopic shift in each band, suggested that only  $\text{Xe}-\text{O}$  bonding was present. Identical Raman spectra were obtained for  $\text{XeO}_2$  samples prepared with either  $\text{H}_2^{16}\text{O}$  or  $\text{D}_2^{16}\text{O}$ , suggesting no hydrogen in the samples; no isotopic shifts of any Raman bands were observed. These chemists were particularly interested in the possibility of  $\text{Xe}-\text{OH}$  units, which was ruled out by the previous observations.

- 8.52 a. The  $[\text{XeF}]^+$  ion, with a total of 14 valence  $s$  and  $p$  electrons, would be expected to have a bond order of 1 (see Section 5.2.1).
- b. Using the VSEPR approach, the following structures can be drawn for the cations of compounds 1-4:



The  $[\text{F}_3\text{NXeF}]^+$  ion, **1**, with a triple bond between sulfur and nitrogen, has the shortest N–S distance (139.7 pm), and  $[\text{F}_5\text{SN}(\text{H})\text{Xe}]^+$ , with a single bond, has the longest distance (176.1 pm). The other ions have bond distances between these extremes that are consistent with double bonds between sulfur and nitrogen.

- c. Compound **1** is expected to have a cation with linear bonding around nitrogen, as shown. However, its crystal structure shows significant bending, with an S–N–Xe angle of

142.6°. This bending is attributed to close N...F contacts within the crystalline lattice.

- d. VSEPR would predict linear bonding with three lone pairs on xenon as, for example, in XeF<sub>2</sub>. The angle measured by X-ray crystallography is 179.6°.
- e. With significant S–N double bonding, these groups are equatorial.
- f. The S–F<sub>axial</sub> bonds are longer, as in many other VSEPR examples (see Figures 3.17 through 3.19). Average distances for these ions are: (2: S–F (axial), 158.2 pm; S–F (equatorial), 152.4 pm) and (3: S–F (axial), 156.1 pm; S–F (equatorial), 151.8 pm).
- 8.53 a.  $D_{2h}$                       c.  $C_1$                       e.  $C_s$   
 b.  $D_{4d}$                       d.  $C_{2v}$                       f.  $C_2$
- 8.54 [FBeNe]<sup>+</sup> The relative order of molecular orbitals may vary depending on the software used. A simple approach, using an extended Hückel calculation, gave the following results:

F–Be bonding

Several orbitals involved:

HOMO: degenerate pair

$\pi$  bonding between Be and F

Next orbital below HOMO

$\sigma$  bonding by the F  $p_z$  and the Be  $s$

Be–Ne bonding

One molecular orbital contributing significantly:

Four orbitals below HOMO

$\sigma$  bonding by the Ne  $p_z$  and the Be  $s$  and  $p_z$

Overall, the interactions between Be and F are stronger than between Be and Ne.

- 8.55 In Xe<sub>2</sub><sup>+</sup>, there are a total of 54 orbitals. We will classify only the higher-energy orbitals here, starting with the highest energy (as calculated using the relatively simple extended Hückel approach). The orbitals used are the 5s, 5p, and 4d.

Molecular Orbital	Type of Interaction	Atomic Orbitals	Molecular Orbital	Type of Interaction	Atomic Orbitals
HOMO	$\sigma^*$	$p_z$	HOMO–8 HOMO–9	$\delta^*$	$d_{x^2-y^2}$ , $d_{xy}$
HOMO–1	$\pi^*$	$p_x$	HOMO–10 HOMO–11	$\delta$	$d_{x^2-y^2}$ , $d_{xy}$
HOMO–2		$p_y$			
HOMO–3	$\sigma$	$p_z$	HOMO–12 HOMO–13	$\pi^*$	$d_{xz}$ , $d_{yz}$
HOMO–4	$\pi$	$p_x$	HOMO–14 HOMO–15	$\pi$	$d_{xz}$ , $d_{yz}$
HOMO–5		$p_y$			
HOMO–6	$\sigma^*$	$s$	HOMO–16	$\sigma^*$	$d_{z^2}$
HOMO–7	$\sigma$	$s$	HOMO–17	$\sigma$	$d_{z^2}$

If this were neutral  $\text{Xe}_2$ , there would be no bond, because every occupied bonding orbital would be offset by an occupied antibonding orbital. In  $\text{Xe}_2^+$ , one electron has been removed, so the bond order is  $\frac{1}{2}$ , making for a long bond. The large atomic radius of Xe further predisposes  $\text{Xe}_2^+$  to having a long bond. It is noteworthy that  $\delta$  bonding is exceedingly weak in this species since the overlap leading to formation of the  $\delta$  and  $\delta^*$  orbitals is very small.

- 8.56** The reference by Steudel and Wong provides illustrations for the four highest occupied molecular orbitals. In addition to the interesting symmetry of these orbitals, the way in which the  $\pi^*$  orbitals of  $\text{O}_2$  are imbedded in the molecular orbitals of  $\text{O}_8$  should be noted.